

FXR activation remodels hepatic and intestinal transcriptional landscapes in non-alcoholic steatohepatitis

Yingquan WEN^{1,2*}, Ziyuan ZOU^{2,3*}, Guanguan ZHAO^{2,4*}, Mengjiao ZHANG⁵, Yongxin ZHANG^{2,6}, Gaihong WANG⁷, Jingjing SHI⁷, Yuanyang WANG^{2,8}, Yeyu SONG^{2,3}, Huixia WANG⁷, Ruye CHEN⁷, Dongxuan ZHENG⁷, Xiaoqun DUAN⁹, Yameng LIU^{2#}, Frank J GONZALEZ¹⁰, Jian-Gao FAN^{3#} & Cen XIE^{1,2,5,6#}

¹*School of Pharmaceutical Science, Nanchang University, Nanchang, 330006, China*

²*State Key Laboratory of Drug Research, Shanghai Institute of Materia Medica, Chinese Academy of Sciences, Shanghai 201203, P.R. China*

³*Center for Fatty Liver, Department of Gastroenterology, Xinhua Hospital Affiliated to Shanghai Jiao Tong University School of Medicine, Shanghai Key Lab of Pediatric Gastroenterology and Nutrition, Shanghai, China*

⁴*Xiangya Hospital, Central South University, Changsha, 410013, P.R. China*

⁵*School of Chinese Materia Medica, Nanjing University of Chinese Medicine, Nanjing 210029, P.R. China*

⁶*University of the Chinese Academy of Sciences, Beijing 100049, People's Republic of China*

⁷*Cascade Pharmaceuticals, Inc, Shanghai, 201321, China*

⁸*Department of Laboratory Medicine and Central Laboratory, Shanghai Tenth People's Hospital, Tongji University, Shanghai, P.R. China*

⁹*Industrial Technology Research Institute of Pharmacy, Guilin Medical University, Guilin, 541199, P.R. China*

¹⁰*Laboratory of Metabolism, Center for Cancer Research, National Cancer Institute, National Institutes of Health, Bethesda, Maryland, USA.*

Author contributions

Y.W., G.Z., M.Z., Y.Z., D.W., J.S., Y.L., H.W., R.C., D.Z. and X.D. performed the experiments. Y.W. and Z.Z. analyzed the RNA-seq data. M.Z. helped with luciferase reporter gene experiment. Y.W., G.Z., Z.Z., H.X and C.X. were responsible for the study concept and design. Y.W. and C.X. wrote the manuscript. C.X., H.X and J.F. supervised the study.

#Correspondence

Cen Xie, State Key Laboratory of Drug Research, Shanghai Institute of Materia Medica, Chinese Academy of Sciences, Shanghai 201203, China. ORCID: <https://orcid.org/0000-0002-4574-8456>. E-mail: xiecen@simm.ac.cn

Jian-Gao Fan, Department of Gastroenterology, Xinhua Hospital Affiliated to Shanghai Jiao Tong University School of Medicine, Shanghai Key Lab of Pediatric Gastroenterology and Nutrition, Shanghai 200092, China. ORCID: <https://orcid.org/0000-0002-8618-6402>. E-mail: fanjiangao@xihuamed.com.cn

Yameng Liu, State Key Laboratory of Drug Research, Shanghai Institute of Materia Medica, Chinese Academy of Sciences, Shanghai 201203, China. ORCID: <https://orcid.org/0000-0003-2970-2308>. E-mail: yameng_liu@simm.ac.cn

Funding

This study was supported by the National Key Research and Development Program of China (2021YFA1301200), Strategic Priority Research Program of the Chinese Academy of Sciences (XDB39020600), National Natural Science Foundation of China (91957116, 82222071, 82104253, 82104261), and Project supported by Shanghai Municipal Science and Technology Major Project.

Abstract

The progression of simple steatosis to non-alcoholic steatohepatitis (NASH) has emerged as a significant health concern. The activation of FXR shows promise in countering this transition and its detrimental consequences. However, the specific alterations within the NASH-related transcriptional network remain elusive, hindering the development of more precise and effective therapeutic strategies. Through a comprehensive analysis of liver RNA-seq data from human and mouse NASH samples, we identified central perturbations within the NASH-associated transcriptional network, including disrupted cellular metabolism and mitochondrial function, decreased tissue repair capability, and increased inflammation and fibrosis, thus shedding light on the complex molecular mechanisms underlying NASH progression. By employing integrated transcriptome profiling of diverse FXR agonists-treated mice, FXR liver-specific knockout mice, and publicly available human datasets, we determined that hepatic FXR activation effectively ameliorated NASH by reversing the dysregulated metabolic and inflammatory networks implicated in NASH pathogenesis. This mitigation encompassed resolving fibrosis, reducing immune infiltration, and creating an immune microenvironment that mirrors the positive trends observed in clinical disease progression. By understanding the core regulatory network of FXR, which is directly correlated with disease severity and treatment response, we identified approximately one-third of the patients who could potentially benefit from FXR agonist therapy. A similar analysis involving intestinal RNA-seq data from FXR agonists-treated mice and FXR intestine-specific knockout mice revealed that intestinal FXR activation attenuates intestinal inflammation, and has promise in attenuating hepatic inflammation and fibrosis. Collectively, our study uncovers the intricate pathophysiological features of NASH at a transcriptional level and highlights the complex interplay between FXR activation and both NASH progression and regression. These findings contribute to precise drug development, utilization, and efficacy evaluation, ultimately aiming to improve patient outcomes.

Keywords: NAFLD/NASH; FXR; Transcriptome; Gut-liver axis; Agonist

1. Introduction

Non-alcoholic fatty liver disease (NAFLD) has become the most common chronic liver disease with a global prevalence of about 25% in the past four decades, and an increase in the prevalence of NAFLD will significantly increase the economic burden ^{1, 2}. NAFLD refers to broad metabolic stressed liver disorders ranging from simple steatosis to its more severe form, non-alcoholic steatohepatitis (NASH), which is marked by excessive fat accumulation, cellular damage, and inflammation with varying degrees of fibrosis ³⁻⁵. NAFLD/NASH is now considered the fastest-growing cause of the end-stage liver diseases, including cirrhosis, liver cancer, and liver failure ⁶⁻⁸. The exact etiology of NASH is still not clear. The multiple-hit hypothesis provides a more accurate and widely accepted view of NASH. Insulin resistance, obesity, ectopic fat deposition, mitochondrial dysfunction, endoplasmic reticulum stress, oxidative stress, inflammation, gut dysbiosis, and genetic factors can all be involved in the development and progression of NASH, and different pathogenic drivers occur in parallel ⁹⁻¹¹. However, the mechanisms governing the transition from the steatotic liver to the advanced NASH and fibrosis are not fully understood ¹².

Despite the growing therapeutic needs, there are no as-yet approved drugs for the treatment of NASH. Current therapeutic targets for NASH mainly involve those mediating lipid, glucose, and bile acid metabolism, inflammation and fibrosis ^{13, 14}. FXR is a bile acid-activated nuclear receptor, which is mainly expressed in the liver and intestine ¹⁵, and has been reported to regulate many biological processes, including bile acid homeostasis and lipid and glucose metabolism ¹⁶. In multiple preclinical models, FXR agonists led to the resolution of NASH through its metabolic and anti-inflammatory effects ¹⁷. The steroid FXR agonist obeticholic acid (OCA), which is licensed as second-line therapy for primary biliary cholangitis, demonstrated the ability to reduce liver fibrosis without worsening of NASH in phase 3 trial and had been considered as a first approval for NASH. However, due to the side effects, including pruritus and elevated LDL cholesterol levels, the FDA did not approve OCA for this indication ¹⁸⁻²¹. Novel non-steroid FXR agonists such as tropifexor (LJN452) and TERN101 have also been developed ^{22, 23}, but they still have similar side effects. Those

side effects are possibly related to the action of FXR itself, suggesting that our understanding of the overall regulatory network of FXR remains inadequate. The lack of systematic studies on the signaling network generated after FXR activation is probably why the development of FXR agonists is unsuccessful.

Deciphering transcriptomic signatures through high-throughput sequencing approaches enables the identification of critical regulatory nodes involved in essential biological functions across diverse tissues and diseases. The development of NASH arises from intricate interactions among metabolic and stress pathways, coinciding with significant alterations in liver transcripts ²⁴. Several studies have indicated that NASH progression is often accompanied by increased inflammation and fibrogenesis, in addition to perturbations in metabolic pathways, but activation of FXR reverses related phenotypes in mice and humans ²⁵⁻²⁷. Therefore, a comprehensive transcriptomic investigation into FXR activation is imperative.

Herein, we initiated a transcriptomic analysis of both human and mouse NASH samples, and discovered critical changes in the regulatory network within healthy to NASH conditions, including dysregulated cellular metabolism, mitochondrial function, and suppressed tissue repair capability in response to damage, together with enhanced inflammation and fibrosis. Notably, we found that hepatic FXR activation effectively reversed all dysregulated networks that propel NASH progression, while intestinal FXR activation exhibited a positive correlation with diminished hepatic inflammation and fibrosis. In addition, we predicted approximately one-third of NASH patients are sensitive to FXR agonist therapy by machine learning. Our study broadens the understanding of the impact of FXR activation on the gut-liver transcriptional regulatory network in NASH and provides insights into the precision therapy of FXR agonists.

Materials and Methods

Animal Studies

Male C57BL/6J mice were purchased from HuaFukang BioScience Company and Vital River Laboratory Animal Technology Co., Ltd. Mice were bred under a specific pathogen-free (SPF) environment, and housed under a 12-hour light/dark cycle with water and food provided *ad libitum*. All experiments were performed according to the Institute of Laboratory Animal Resources guidelines and approved by the Institute Animal Care and Use Committees at Shanghai Institute of Materia Medica or Cascade Pharmaceuticals, Inc. Male C57BL/6J mice were purchased from HuaFukang BioScience Company. Male mice from 7-8 weeks old were fed low-fat diet (LFD, 10% fat) or GAN diet (40% kcal fat, 20% kcal fructose and 2% cholesterol; D09100310 from Research Diet Inc, USA) for 6 weeks or GAN diet plus CCl₄ (CCl₄: corn oil =1:19, 2 µl/g body weight) together with vehicle or FXR agonists (30mg/kg OCA, 0.1mg/kg LJN452 and 100mg/kg TERN101) for additional 4 weeks. The mice were sacrificed 48 h after the final CCl₄ injection and the samples were collected for follow-up analysis. Intestinal *Fxr*-null (*Fxr*^{ΔIE}), hepatic *Fxr*-null (*Fxr*^{ΔHep}), and the control *Fxr*^{f/f} mice were described previously ²⁸. Male 7-8 weeks old *Fxr*^{f/f}, *Fxr*^{ΔHep} and *Fxr*^{ΔIE} mice on chow diet were treated with OCA (20 mg/kg/day) 2, 24 and 48 h before sacrificing.

Liver and Serum Analysis

Livers were collected and quickly frozen in liquid nitrogen and subsequently stored at -80°C for analysis. Serum was collected and centrifuged at 3,500 rpm for 15 min, and supernatant was collected and stored at -80°C. Liver triglycerides, cholesterol and HYP, as well as serum triglycerides, total cholesterol, HDL-C, LDL-C, ALT, AST, TBIL and DBIL were measured following commercially available kit protocols (Jiancheng, Nanjing, China).

Histological Analysis

Sections of liver samples fixed in 10% formaldehyde aqueous solution and embedded in paraffin were stained with hematoxylin and eosin (H&E) and stained with Sirius red for collagen deposition and Oil Red O stain for frozen sections. Blind histological scoring of liver sections according to criteria (including steatosis, lobular inflammation, and ballooning)

²⁹. Sections stained with Sirius red were analyzed to obtain fibrosis scores according to the criteria. Images were taken with an upright microscope and quantitative data were taken with ImageJ software (v1.53).

Quantitative Real-time PCR

Mouse liver and ileum were frozen in liquid nitrogen and stored at -80°C. Total RNA from frozen tissues was isolated and extracted by standard phenol-chloroform with Trizol reagent. cDNA was synthesized from 2 µg of total RNA with PrimeScript reverse transcriptase (Takara Bio). Quantitative real-time polymerase chain reactions (PCRs) were performed with SYBR Premix Ex Taq (Takara Bio) and a real-time PCR detection system. Gene expression levels were calculated using the comparative method ($2^{-\Delta\Delta Ct}$) and presented as relative expression. The real-time PCR primer sequences are summarized in **Supporting Table S1**.

Public Datasets of Human

The publicly available dataset E-MAXP-3291 was downloaded from the Array Express (<https://www.ebi.ac.uk/arrayexpress/>), which comprised clinically defined 45 patients, Normal ($n = 19$), Steatosis ($n = 10$) and NASH ($n = 16$), and GSE48452 was downloaded from GEO (gene expression omnibus, <https://www.ncbi.nlm.nih.gov/geo/>) database. This study assayed the genome-wide mRNA levels in hepatic tissue samples with Affymetrix GeneChip® Human 1.0ST arrays. In our study, different genes expression analysis was performed between control, steatosis ($n = 6$), and NASH ($n = 3$)³⁰.

The publicly available datasets GSE135251 was screened and downloaded from the GEO (gene expression omnibus, <https://www.ncbi.nlm.nih.gov/geo/>) database. To further evaluate the inflammation and fibrosis status after treatment with the 3 FXR agonists, the expression profile of high throughput sequencing of 216 snap-frozen liver biopsies samples: GSE135251 was downloaded for GSEA and ssGSEA, which comprised controls ($n = 10$), NAFL ($n = 51$) and NASH with fibrosis stages of F0/1 ($n = 34$), F2 ($n = 53$), F3 ($n = 54$) and F4 ($n = 14$). Normalized and logarithmic converted expression of different disaster biopsies was

calculated by using the limma relative log expression normalization method. In addition, outliers that express abnormal amounts were removed, and batch effects were corrected (R package “*svg*”).

Isolation of RNA and Library Preparation for RNA-seq

RNA purification, reverse transcription, library construction, and sequencing were performed by Shanghai Majorbio Bio-pharm Biotechnology Co., Ltd. (Shanghai, China) according to the manufacturer’s instructions (Illumina, San Diego, CA).

Quality Control and Read Mapping

The raw paired-end reads were trimmed and quality controlled by fastp with default parameters. Then, clean reads were separately aligned to the reference genome with orientation mode using HISAT2 software ³¹. The mapped reads of each sample were assembled by StringTie in a reference-based approach. Probes were transformed and duplicate genes were removed.

Analyses of RNA-seq Data

Normalized and logarithmic converted expression of mouse genes (FPKM) by using limma relative log expression normalization method. Then, a principal component analyses (PCA) analysis was performed to demonstrate a large degree of differentiation between each group for further analysis. Normalized RNA-seq data was used for a heatmap of gene expression (<https://www.omicstudio.cn/home>). Furthermore, normalized and logarithmic converted RNA-seq data was used for PCA analysis and others. Software R (version 4.1.2) and the limma R package were used for differential gene expression analysis. The thresholds of differentially expressed genes (DEGs) were all set as $p < 0.05$ and $|\log_2(\text{fold-change})| > 0$.

Enrichment Analysis

The DEGs generated by the limma package were used as the input. Gene Ontology (GO) and

Kyoto Encyclopedia of Genes and Genomes (KEGG) pathway enrichment analyses were performed using the clusterProfiler R package. The analysis used a strict cutoff of P values and an false discovery rate (FDR) both are lower than 0.05. Top GO and KEGG terms were displayed.

Protein-Protein Interaction Network Analysis

Protein-protein interactions (PPIs) were analyzed using STRING (<https://string-db.org/>), an online database of known and predicted protein-protein interactions. The protein-protein interaction information derived from the STRING database was then uploaded into Cytoscape (version 3.8.2) to visualize further and construct the PPI network. The algorithm betweenness calculated the top 30 genes that are strongly related and have more interactions with neighboring nodes, while the color shades of the nodes indicated the abundance of protein interactions.

Gene Set Analysis

Gene Set Enrichment Analysis (GSEA) was performed on limma normalized and log transformation expression values of genes derived from liver samples of NASH human and mouse ³². To further explore the improvement of fibrosis status after treatment with 4 FXR agonists. We performed homozygous gene conversion on mouse RNA-seq data and compared gene expression profiles with 216 human liver biopsy samples (grouped by fibrosis stage). Analysis of pathways and genes involved in fibrosis was performed using the Nanostring nCounter Fibrosis v2 Panel ³³. The Normalized Enrichment Score (NES) was calculated to enable a comparison between human and mouse pathway enrichment. Mouse and human data used their respective healthy groups as control phenotypes. Additionally, single sample GSEA (ssGSEA) was performed using normalized and log-transformed human and mice gene expression data, in which batch effects were removed for comparison. Furthermore, we continue to explore inflammation by using the inflammatory pathways associated with fibrosis described in the Nanostring nCounter Fibrosis v2 Panel, exploring

inter-sample correlation using Euclidean distance and Pearson correlation.

Immune Cell Infiltration Analysis

Immune infiltration in the liver was analyzed using ssGSEA, based on non-overlapping gene sets representing 28 immune infiltrating cells, with negative values removed and the level of immune infiltration within the group taken as the mean value. t-test was performed with 3 FXR agonists and NASH group, P value < 0.05 is considered a significant difference. A total of 22 types of immune infiltrating cells were evaluated in the liver, to get comprehensive information about the immune cells expression situation. The code for CIBERSORT and the standard immune cell expression file "LM22.txt" were obtained from the official website (<https://cibersort.stanford.edu/>). The proportion of immune cell members in mixed cell populations was assessed using a stack diagram.

Cell Communication Analysis by Nichenet

We first performed a single-cell localization analysis of FXR core downregulated genes, determined which receptors are distributed on the NPC, and further identified the corresponding ligand information for the receptor. Interactions between ligand and receptor were found from lr_network.rds³⁰. NicheNet (v0.1.0) was used to rank the ligands based on how accurately they predicted if a gene belonged to a gene set of interest compared to a background gene set³⁴. A ligand-receptor potential score was calculated that reflected the weight of the interaction between the ligand and receptor in the weighted ligand signaling network from weighted_networks.rds.

Statistics

Statistical analyses were performed using GraphPad Prism (version 9.0.0, GraphPad). All experimental values were presented as mean ± SEM. Statistical significance between two groups was determined using a two-tailed Student's *t*-test. One-way ANOVA followed by Tukey's post hoc correction was applied for multi-group comparisons. p<0.05 was considered

to be significant. The correlation analysis was investigated using Pearson's test (two-sided).

Results

Characterization of global transcriptomic features across humans and mice during NASH progression

To explore which critical biological processes are altered in the progression of NASH, we analyzed the transcriptional changes using two public RNA-seq datasets of NAFLD patients (GSE48452 and GSE130970). Principal component analyses (PCA) showed that the livers from healthy controls, simple steatosis, and NASH patients were separated in PC1 (Figure 1A). Furthermore, k-means clustering of genes that were differentially expressed in two human datasets revealed 4 clusters (C1, C3, C5, and C7) were upregulated, and 4 clusters (C2, C4, C6, and C8) were downregulated in NASH patients (Figure 1B). Both KEGG and GO Pathway analysis demonstrated that genes induced in clusters C1 and C5 were assigned to inflammation-related pathways, such as cytokine-cytokine receptor interaction, toll-like receptor signaling, NF- κ B signaling, and immune cell migration, chemotaxis, and response to external stimulus. Meanwhile, the genes induced in clusters C3 and C7 were related to tissue injury and fibrogenesis, including DNA replication, extracellular matrix (ECM) receptor interaction, focal adhesion, ECM organization and assembly, and autophagy (Figure 1C, D). Most of the genes repressed in NASH (C2, C4, C6, and C8) were assigned to small molecule catabolic processes, mitochondrial respiration-related pathways, as well as tissue regeneration-related signalings and processes, such as membrane potential, cell fate specification, Notch and Wnt signaling, and RNA processing and splicing (Figure 1C, E). These results revealed that the core pathogenetic factors in NASH patients included increased tissue injury, inflammation, and fibrogenesis, but dysregulated small molecule and energy metabolism, impaired mitochondrial function, and suppressed tissue repair.

To explore the conservativeness of pathways variation in NASH between humans and mice, we established two different NASH mouse models, including the Gubra-Amylin NASH (GAN) diet induced NAFL and NASH, and GAN diet plus CCl₄-induced NASH with

advanced fibrosis (Figure 2A). Mice in both NASH models showed more severe lipid accumulation, inflammation and fibrosis (Figure 2B and S1A). Next, we performed RNA-seq on the livers of mice from the above models. PCA showed that the livers of control, NAFL and NASH mice from two different models were clearly separated in PC1 (Figure 2C). Furthermore, k-means clustering of genes that were differentially expressed revealed 3 upregulated clusters (C1, C3, and C5) and 3 downregulated clusters (C2, C4, and C6) in both NASH models (Figure 2D). Pathway analysis demonstrated that genes induced specifically in NASH (C1, C3, and C5) mainly enriched in focal adhesion, chemokine signaling pathway and ECM receptor interaction, as well as extracellular matrix (ECM) organization, actin filament, leukocyte migration and platelet activation, all of those are related to inflammation and fibrosis (Figure 2E). Genes repressed in NASH (C2, C4, and C6) were attributed to small molecule catabolic processes, mitochondrial function, and tissue repair-related pathways, such as Wnt signaling, RNA processing, epigenetic modification, and cell cycle (Figure 2F). Overall, the pathway analysis revealed that the cellular metabolism, mitochondrial function were obstructed and the repair function in response to cell damage was hindered during NASH progression in mice, accompanied by the development of inflammation and fibrosis.

Cellular metabolism, mitochondrial function, and tissue repair-related pathways were enriched in both mouse and human downregulated clusters, while the upregulated pathways were enriched in immune regulation and fibrogenesis, and showed a characteristic upregulation when NAFL progressed to NASH. These data suggest that mouse NASH models can represent human NASH (Figure S1B). Therefore, intervention targeting the above disrupted pathways (defined as core NASH transcriptional network) in both humans and mice could be a potential therapeutic strategy for NASH, and we can use mouse studies to interpret the pharmacologic consequences of FXR agonists on NASH in humans.

FXR agonist treatment ameliorates the development of NASH

In recent years, the research and development of FXR agonists have entered a period of rapid development, but limited clinical benefits and serious side effects have restricted their

applications. Therefore, it is crucial to further understand the core regulatory network of FXR agonists in NASH. OCA is the first steroid FXR agonist to reach clinical endpoints. LJN452, TERN101 are non-steroidal compounds further developed to circumvent the hormone-like side effects of OCA. Different FXR agonists can effectively eliminate the influence of the off-target effects of the compounds themselves, which will help us follow up with better systematic research on the core regulatory network of FXR in NASH.

We evaluated the therapeutic effects of OCA, LJN452 and TERN101 on the GAN diet plus CCl₄-induced NASH with advanced fibrosis (Figure 3A). There was no significant difference in body weight between NASH mice and superimposed FXR agonists treated mice (Figure 3B), but FXR agonist treatment increased liver weights. Liver triglyceride and HYP levels, but not cholesterol, were significantly reduced after treatment with FXR agonists (Figure 3C). Treatment with LJN452 and TERN101 reduced serum triglyceride and cholesterol levels and serum HDL-C and LDL-C. In addition, the FXR agonists decreased TBIL, DBIL, liver injury markers, ALT, and AST (Figure 3D). We also tested the mRNA expression of FXR target genes by qRT-PCR and found that FXR agonists significantly reduced the expression of *Cyp7a1* and *Cyp8b1* in the liver, and increased the expression of *Fgf15* and *Shp* in the intestine (Figure 3E), confirming the activation of both hepatic and ileal FXR signaling by these agonists. Liver histology analysis revealed a significant reduction in steatosis, inflammation and fibrosis (Figure 3F,G). These results suggest that treatment with FXR agonists has an ameliorative effect on NASH as previously reported.

FXR activation reverses the dysregulated core NASH transcriptional network

To elucidate the hepatic FXR-activated transcriptional network in NASH, we performed RNA sequencing on the livers of NASH mice treated with FXR agonists (OCA, LJN452 and TERN101). Additionally, to accurately identify the transcripts influenced by FXR, we also conducted a parallel analysis on the livers of mice with hepatocyte-specific FXR deficiency (*Fxr*^{ΔHep}) and their control counterparts (*Fxr*^{f/f}), both subjected to OCA treatment to augment the FXR-dependent signaling (Figure 4A). PCA displayed a clear separation between liver

transcripts of NASH mice treated with vehicle and those with FXR agonists; similarly, distinct separation was observed between the liver transcripts of OCA-treated *Fxr^{f/f}* and *Fxr^{ΔHep}* mice (Figure 4B). Through a rigorous DEGs analysis, we identified four sets of genes that exhibited differential expression (Figure 4C and S2A). By intersecting these sets, we discovered two groups of FXR-dependent genes comprising 210 genes that were consistently upregulated and 218 downregulated genes in response to FXR activation (Figure 4D). The pathway enrichment analysis of the 210 upregulated genes, along with Gene Set Enrichment Analysis (GSEA) applied to the entire transcriptomes, unveiled significant upregulation of cellular metabolism and mitochondrial function-related pathways following FXR agonist treatment, which were found dysfunctional in core NASH pathways. Conversely, the pathways enrichment analysis of the 218 downregulated genes and GSEA results demonstrated a marked reduction in inflammation and fibrosis-related pathways, which were recognized as a pathogenic signature in NASH progression, were downregulated in FXR agonist-treated mice (Figure 4E,F and Figure S1B). Notably, FXR agonist treatment appears to exert a dual effect by promoting the upregulation of beneficial pathways linked to cellular metabolism, mitochondrial function, RNA processing, while concurrently dampening the activity of detrimental inflammation and fibrosis-related pathways in core NASH transcriptional network. We also compared the different transcriptomes between steroidal FXR agonist OCA and non-steroidal FXR agonists, and found that non-steroidal agonists (LJN452 and TERN101) showed more significant cholesterol metabolism but weaker lipid metabolism, relative to OCA (Figure S2B,C).

Collectively, our data proves that hepatic FXR activation holds the capacity to reverse the dysregulated core NASH transcriptional network. This intricate modulation underscores the potential of FXR as a versatile therapeutic target with relevance across a spectrum of core pathways implicated in the pathogenesis of NASH.

Machine learning predicts patients' response to treatment of FXR agonists

Strong heterogeneity of NASH significantly influences the efficacy of FXR agonists, and

patients within the same NASH stage responded differently to FXR agonist therapy. We sought to hypothesize the response of patients to FXR agonist therapy through the heterogeneity of their genes expression. We performed Protein-Protein Interaction (PPI) analysis to discover the core gene network regulated by FXR. The PPI network diagram focusing on the top 30 FXR core upregulated genes, highlighted the strong negative correlation between *Upb1*, *Mt-Md3*, *Aox3*, *Mcee*, *Dpp4* and *Maob* with liver TG, indicating the involvement of these genes in resolving steatosis by FXR activation (Figure 5A,B). Furthermore, the top 30 FXR core downregulated genes were strongly positive-correlated with ALT and AST, confirming the ability of FXR agonists to ameliorate NASH-associated liver injury (Figure 5C,D). To validate these 60 FXR-regulated genes are associated with the NASH progression in humans, three machine learning algorithms were employed on dataset GSE135251³⁵: random (RF), support vector machine (SVM), and logistic regression (Logi). The receiver operating characteristic (ROC) curves revealed that these FXR core regulated genes could successfully predict the NASH patients from NAFLD patients (Figure 5E).

To narrow down the NASH-related and FXR core regulated gene set, and to further identify the NASH patients sensitive to FXR agonists therapy, least absolute shrinkage and selection operator (LASSO) regression analysis was used. The features with a higher importance score indicate a more substantial contribution of the genes in the prediction model. We then ranked the genes by their importance (impurity) scores, and the top 11 and top 16 genes are respectively shown (Figure 5F,G). NASH patients with the opposite expression pattern of these 27 genes are thought to respond better to the treatment with FXR agonists potentially. ssGSEA was used to differentiate NASH patients based on the normalized enrichment score (NES) of the corresponding FXR core regulated gene set (Figure 5H,I). Similarly, ROC curves showed great predictive properties of these 27 genes for disease (Figure 5J). The intersection section shows that approximately 28.64% of the NASH patients exhibited more significant alterations of FXR core-regulated network, and thus these patient might be more sensitive to FXR treatment represent (Figure 5K,L). The results suggest that the efficacy of FXR agonists in the early stages of NASH may be suboptimal and that they

might act better in the late stages of NASH fibrosis, highlighting the need for more precise drug development, utilization, and efficacy assessment.

FXR activation mitigates liver inflammation and fibrosis mainly via liver non-parenchymal cells

NAFLD is a pro-inflammatory disorder, wherein liver inflammation with chronic hepatic injury and the resulting fibrosis play pivotal roles in orchestrating the transition from NAFL to NASH³⁶. To elucidate the clinical impact of transcriptional modifications following FXR agonist treatment, we conducted a comparative analysis between RNA-seq data from experimental mice and corresponding orthologous genes derived from 216 human liver biopsy samples, categorized by fibrotic stage³⁵. Hierarchical clustering of liver samples from humans and mice revealed two distinct groups displaying differential enrichment for pre-fibrotic or fibrotic disease stages (Figure 6A). PCA highlighted that the progression from NAFL to F4 stage in humans and from control to NASH in mice is primarily orchestrated by PC1. Moreover, livers from FXR agonist-treated mice closely clustered around the center of F2 ellipsoid (Figure 6B). To determine the similarity in fibrosis-related pathways between mice and humans, we computed normalized enrichment scores. Analysis of FXR core downregulated pathways unveiled the suppression of fibrosis-related processes post FXR agonist treatment, including cell-substrate adhesion, collagen fibril organization, collagen metabolic process, and fibroblast proliferation (Figure 6C). We also performed GESA on genes involved in fibrosis pathways using the Nanostring nCounter Fibrosis v2 Panel³³. Among the 17 significantly altered pathways in FXR agonist-treated mice, those in cluster II were predominantly repressed by FXR activation, including critical processes integral to NASH pathophysiology, such as focal adhesion kinase, PDGF signaling, ECM synthesis, collagen biosynthesis and modification (Figure 6D). Both Pearson correlation and Manhattan distance analyses indicated that FXR agonist-treated mice are more remarkably similar to F0-F1 biopsies, distinct from other fibrosis stages and most dissimilar to F4 stage biopsies (Figure 6D and S3A). Regarding specific fibrosis pathways, single-sample GSEA (ssGSEA)

³² exhibited downregulation of pathways in cluster II and III compared to NASH mice or individuals in the most advanced human NASH stage, F4. The heatmap depicting gene expression underscored that FXR agonist treatment significantly curtailed the expression of several fibrosis and NASH progression markers (*COL1A1*, *COL1A2*, *COL3A1*, *COL4A21*, *COL4A2*, *COL5A1*, *COL5A3*, *COL6A3*, *COL14A1*, *COL16A1*, *MMP2* and *TGFB1*) to levels on par with or below those observed in mice fed a control diet and NAFL patients (Figure 6E and S3B). These data provide valuable insights into the cross-species similarities in fibrogenesis and common therapeutic response to FXR agonists.

The immune microenvironment undergoes crucial alterations in the development of NASH, with inflammation-induced liver damage contributing to fibrosis progression. To explore the shifts in the immune infiltration landscape post FXR agonist treatment, we performed GSEA on inflammatory pathways closely intertwined with fibrosis using the Nanostring nCounter Fibrosis v2 Panel. Upon FXR agonist treatment, some pro-inflammatory pathways were repressed, most notably type I and II interferon responses, phagocytosis, chemokine and cytokine signaling, granulocyte degranulation, adenosine pathway, and TLR signaling pathway (Figure 6F). Furthermore, we investigated alterations in specific immune cell populations after FXR agonist treatment, and found that central memory CD4⁺ T cells, immature dendritic cells, and natural killer cells exhibited significant downregulation post FXR agonist treatment (Figure S3C). To better understand the immune cell dynamics, we employed CIBERSORT to calculate immune infiltration deconvolution scores for each sample ³⁷. Similarly, the results revealed that in NASH mice, the fraction of resting dendritic cells, monocytes and regulatory T cells increased, while the fraction of naive B cells and plasma cells decreased in comparison to healthy mice (Figure S3D). Our findings elucidate the intricate immunomodulatory effects of FXR agonist treatment in NASH. By downregulating pro-inflammatory pathways and modulating specific immune cell subsets, FXR activation showcases its potential in shaping the immune landscape, further contributing to fibrosis alleviation and inflammation mitigation.

Next, we investigated the cellular localization of the 180 core downregulated genes at the

single-cell level, and identified 9 genes were mainly expressed in liver non-parenchymal cells (NPCs), such as macrophages, T cells and fibroblasts. Some of them have been previously established as causal factors in fibrosis progression, including vascular cell adhesion molecule-1 (*Vcam1*), AXL receptor tyrosine kinase (*Axl*), complement C3a receptor 1 (*C3ar1*) and integrin subunit beta 2 (*Itgb2*)³⁸⁻⁴¹. NicheNet analysis incorporated ligand-target gene interaction data on these genes was then conducted to depict their roles in intra-hepatic crosstalk between hepatocytes and NPCs. The nine FXR agonists-induced genes as receptors in NPCs were predicted to have several ligand genes in hepatocytes (Figure 6G and S3E). The results of the pathway enrichment analysis showed that some genes are involved in processes related to fibrosis such as cell-matrix adhesion (*Fga*, *Agt* and *Vegfa*) and blood coagulation (*Plg*, *Apoe*, *Fga*, *F2*, *Kng1*, *C3* and *Pros1*). These results highlight the importance of hepatic NPCs in mediating FXR agonist-induced effects on inflammation and fibrosis. The intricate interplay between these genes, hepatocyte-derived ligands, and the hepatokine network offers a novel perspective on the multifaceted impact of FXR activation.

Thus, the suppression of key inflammation and fibrosis-related processes, as well as modulation of different cells in the microenvironment substantiates the potential of FXR agonists in alleviating NASH.

Intestinal FXR activation alleviates NASH through the gut-liver crosstalk

To discover the intestinal transcriptional network activated by FXR in the context of NASH, we conducted RNA-seq on samples from NASH mice treated with FXR agonists; at the meantime, we also analyzed the samples from OCA-treated enterocyte-specific FXR deficiency (*Fxr^{ΔIE}*) and control (*Fxr^{ff}*) mice to identify the transcripts influenced by intestinal FXR (Figure 7A). PCA analysis distinctly segregated NASH mice and those treated with different FXR agonists along PC1, as well as OCA treated *Fxr^{ff}* and *Fxr^{ΔIE}* (Figure S4A). We obtained four sets of DEGs, and the recognized FXR target gene *Fgf15* among the corresponding up or downregulated genes confirmed the reliability of the RNA-seq data (Figure S4B). By intersecting these sets, we identified 55 FXR-dependent upregulated genes

and 143 downregulated genes (Figure 7B and S4C). The pathway enrichment analysis of 55 upregulated genes indicated increased lipid biosynthesis and metabolism, bile acid secretion and transport in the intestine (Figure 7C). Conversely, the pathway enrichment analysis of 143 downregulated genes pointed to significant downregulation of inflammation-related pathways, including B cell activation, proliferation and differentiation, and leukocyte, lymphocyte and mononuclear cell proliferation (Figure 7D), implying a marked shift in intestinal immunity. To better depict the intestinal ecology in NASH and understand the effect of FXR activation, we performed GSEA to compare the transcriptional profiles of NASH mice with healthy mice and FXR-agonist treated mice. Compared to the healthy controls, bile acid-related pathways were downregulated, while inflammation-related pathways were upregulated in NASH mice. Moreover, FXR agonists reversed the dysregulated pathways in the intestine induced by NASH (Figure 7E). Our data support the notion of an improved intestinal ecology following FXR activation.

Next, we then shifted our focus to understanding the influence of FXR agonists on the liver via the gut-liver axis in the NASH mice. First, we performed DEG analysis for the livers from *Fxr^{f/f}* vs *Fxr^{ΔIE}*, Control vs NASH (GAN diet), and Control vs NASH (GAN diet + CCl₄) (Figure 7F). These transcriptional alterations in the liver subsequent to intestinal FXR deficiency or activation are closely associated with NASH progression. Both FXR activation and inhibition in the intestine have been reported to produce metabolic benefits on NAFL or NASH^{16, 42}. We adopted four intersection strategies to uncover the potential benefits of intestinal FXR agonists or inhibitors (Figure 7G). Pathways analysis of 35 and 23 genes (FXR inhibitor benefit) demonstrated that FXR inhibition increased autophagy and reduced DNA damage and cell death (Figure 7H). In addition, pathways analysis of 158 and 86 genes (FXR agonists benefit) revealed that intestinal FXR activation leads to decreased inflammation and fibrosis and enhanced energy metabolism (Figure 7I and S4D). In conclusion, intestinal FXR activation may work independently of the regulatory network centered on intestinal FXR inhibition, but both contribute to the resolution of NASH through the gut-liver axis.

Discussion

NASH is recognized as an essential contributor to hepatitis, cirrhosis, hepatocellular carcinoma, and cardiovascular events, which underscores the urgent need to understand the mechanisms of NASH and develop an effective treatment⁴³. FXR belongs to the nuclear receptor superfamily and is highly expressed in the liver and intestine. Targeting FXR represents a promising therapeutic approach to NASH. In recent years, many studies have implicated the metabolic benefits of FXR activation in NASH⁴⁴, and multiple FXR agonists have entered clinical trials such as OCA, LJN452 and TERN101. However, the mechanisms for the beneficial effects of FXR agonists have not been fully elucidated. Therefore, it is imperative to understand the FXR-centered regulatory network in the liver and intestine, as well as the gut-liver crosstalk. In the current study, we demonstrated that hepatic FXR agonists alleviate NASH associated phenotypes and produce a wide range of metabolic benefits, including improved cellular metabolism of amino acids, fatty acids, and carboxylic acids and mitochondrial function, as well as inflammation and fibrosis⁴⁵. Alterations in these FXR-centered pathway networks in the liver play a critical role in NASH remission. The machine learning results further suggest that the population sensitive to FXR agonists therapy is approximately one-third of total NASH patients. In addition, FXR is highly expressed in the intestine, which works with hepatic FXR to control the enterohepatic circulation of bile acids and maintains metabolic homeostasis. These results expand our understanding of the mechanism of action of FXR agonists and their applications.

Using different RNA-seq datasets, we demonstrate that NASH mice and humans share similar core NASH transcriptional networks. Unsupervised clustering was performed on transcriptomic data from two batches of NASH mice and two datasets representing three different NAFLD stages (healthy, steatosis, and NASH) in humans. Early in NASH, DNA replication and signal transduction are enhanced to repair tissue damage. However, RNA processes are inhibited, suggesting that transcriptional and translational processes are blocked and accompanied by dysregulated small molecule and energy metabolism and mitochondrial

dysfunction. Prolonged tissue damage increases immune cell infiltration and fibrocollagenous tissue, further exacerbating liver injury. That vicious cycle drives the progression of NASH. Activation of FXR by different agonists, OCA, LJN452, and TERN101, has been shown to reverse the dysregulated NASH transcriptional network similarly. However, the PCA results indicated a strong separation due to the structural differences between these FXR agonists, suggesting different action modes between different agonists (steroidal or nonsteroidal structure, and even within nonsteroidal compounds). The side effects of these FXR agonists remain unresolved and require further study. Nonetheless, the ameliorative effects of these FXR agonists on hepatic lipid accumulation, injury, inflammation, and fibrosis in NASH are definite⁴⁶.

A characteristic of NASH is hepatic inflammation, which is believed to drive fibrosis development⁴⁷. Treatment with FXR agonists downregulates inflammation-related pathways, including interferon production, phagocytic cell function, TLR signaling, and neutrophil degranulation, which are known to be involved in NASH pathogenesis. Subsequent GSEA analyses reveal downregulated pathways involving collagen biosynthesis, ECM synthesis, and focal adhesion kinase, leading to significant reductions in fibrosis markers comparable to control mice or healthy human livers. These data suggest that hepatic FXR activation remodels the hepatic immune microenvironment and may directly affect immune cells other than hepatocytes. Further examination of FXR core downregulated genes showed that receptors regulated by FXR agonists, such as macrophages, T cells, and fibroblasts, were found on NPCs. Notably, among others, AXL, VCAM1, ITGB2, and C3AR1 have been associated with inflammation and fibrosis.

Activation of intestinal FXR was reported to improve hepatic glucolipid metabolism⁴⁸. However, several studies showed that specific knockout or selective inhibition of intestinal FXR improved obesity-related metabolic dysfunction, including NASH^{42,49-52}. Therefore, intestinal FXR may act as a bidirectional liver metabolism and function regulator. Our study reveals that intestinal FXR activation is associated with decreased hepatic inflammation and fibrosis, while intestinal FXR antagonism is linked to enhanced autophagy and ameliorated

cell death in the liver.

A recent 18-month clinical trial showed that 22.4% of participants receiving once-daily oral OCA 25 mg achieved a ≥ 1 stage improvement of fibrosis with no worsening of NASH⁵³. Similar to our predicted proportion of the population sensitive to FXR agonist treatment. In the early stages of NASH, the proportion of the population susceptible to FXR agonist treatment is low. This may be because FXR agonists produce a wide range of metabolic benefits but have nonspecific effects on lipid accumulation and inflammation. These results suggest that our use of FXR agonists in early NASH is not appropriate. FXR has too many target genes in the organism, and some of the target genes related to the action of FXR have yet to be discovered, while the specific pathways by which FXR acts on some of the target genes are unclear. The core regulatory network of FXR that we have given deserves further investigation, which may provide new targets for drug development in NASH.

In summary, given the complex physiological effects of FXR activation, including various intractable side effects, exploring the core regulatory network can help us perform more precise drug development, utilization, and efficacy evaluation. The excavation and development of new targets may provide new insights into the treatment of NASH. Meanwhile, the visualization of the coregulatory network also provides a new transcriptomic perspective for evaluating new drug efficacy.

ACKNOWLEDGEMENTS

We thank Kanglong Wang, Pengxiang Mu, and Cuina Li for their help with animal dissection and sample collection.

REFERENCES

1. Younossi, Z. M.; Koenig, A. B.; Abdelatif, D.; Fazel, Y.; Henry, L.; Wymer, M., Global epidemiology of nonalcoholic fatty liver disease—Meta-analytic assessment of prevalence, incidence, and outcomes. *Hepatology* 2016, 64 (1), 73-84.
2. Powell, E. E.; Wong, V. W.-S.; Rinella, M., Non-alcoholic fatty liver disease. *The Lancet* 2021, 397 (10290), 2212-2224.

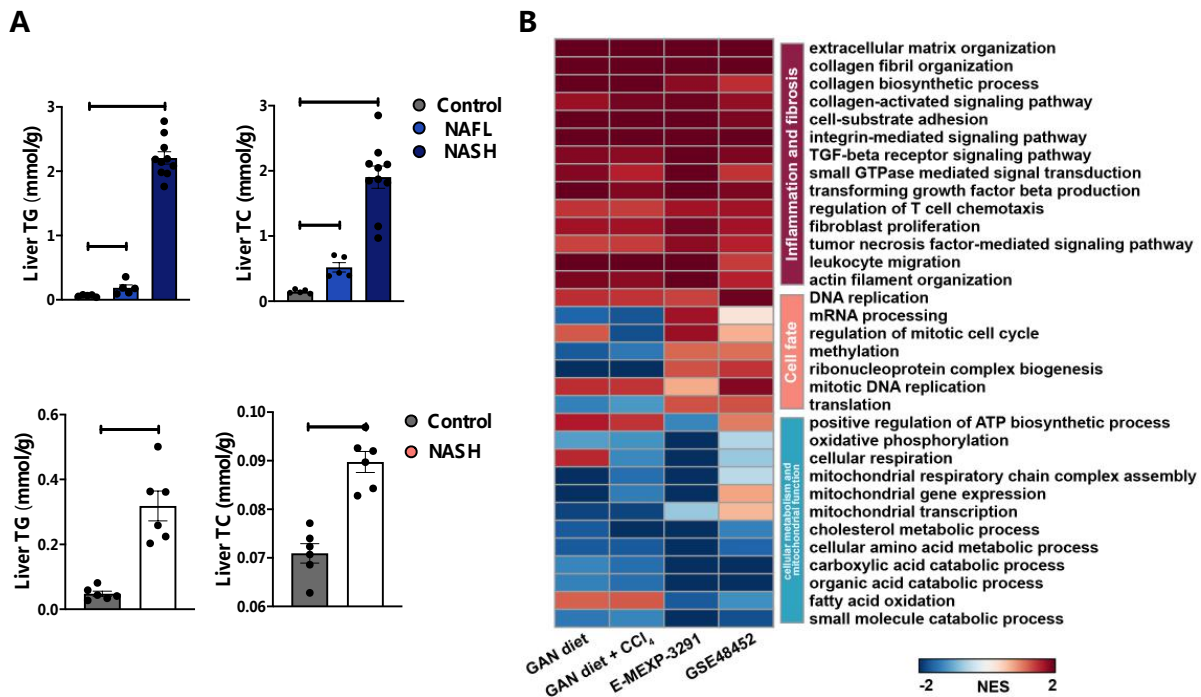
3. Younossi, Z. M.; Henry, L., Fatty Liver Through the Ages: Nonalcoholic Steatohepatitis. *Endocrine Practice* 2022, 28 (2), 204-213.
4. Pouwels, S.; Sakran, N.; Graham, Y.; Leal, A.; Pintar, T.; Yang, W.; Kassir, R.; Singhal, R.; Mahawar, K.; Ramnarain, D., Non-alcoholic fatty liver disease (NAFLD): a review of pathophysiology, clinical management and effects of weight loss. *BMC Endocr Disord* 2022, 22 (1), 63.
5. Saiman, Y.; Duarte-Rojo, A.; Rinella, M. E., Fatty Liver Disease: Diagnosis and Stratification. *Annu Rev Med* 2022, 73, 529-544.
6. Younossi, Z.; Stepanova, M.; Ong, J. P.; Jacobson, I. M.; Bugianesi, E.; Duseja, A.; Eguchi, Y.; Wong, V. W.; Negro, F.; Yilmaz, Y.; Romero-Gomez, M.; George, J.; Ahmed, A.; Wong, R.; Younossi, I.; Ziayee, M.; Afendy, A.; Global Nonalcoholic Steatohepatitis, C., Nonalcoholic Steatohepatitis Is the Fastest Growing Cause of Hepatocellular Carcinoma in Liver Transplant Candidates. *Clin Gastroenterol Hepatol* 2019, 17 (4), 748-755 e3.
7. Burra, P.; Becchetti, C.; Germani, G., NAFLD and liver transplantation: Disease burden, current management and future challenges. *JHEP Rep* 2020, 2 (6), 100192.
8. Estes, C.; Razavi, H.; Loomba, R.; Younossi, Z.; Sanyal, A. J., Modeling the epidemic of nonalcoholic fatty liver disease demonstrates an exponential increase in burden of disease. *Hepatology* 2018, 67 (1), 123-133.
9. Koo, J. H.; Han, C. Y., Signaling Nodes Associated with Endoplasmic Reticulum Stress during NAFLD Progression. *Biomolecules* 2021, 11 (2).
10. Buzzetti, E.; Pinzani, M.; Tsochatzis, E. A., The multiple-hit pathogenesis of non-alcoholic fatty liver disease (NAFLD). *Metabolism* 2016, 65 (8), 1038-48.
11. Petrescu, M.; Vlaicu, S. I.; Ciupercean, L.; Milaciu, M. V.; Marginean, C.; Florea, M.; Vesa, S. C.; Popa, M., Chronic Inflammation-A Link between Nonalcoholic Fatty Liver Disease (NAFLD) and Dysfunctional Adipose Tissue. *Medicina (Kaunas)* 2022, 58 (5).
12. Friedman, S. L.; Neuschwander-Tetri, B. A.; Rinella, M.; Sanyal, A. J., Mechanisms of NAFLD development and therapeutic strategies. *Nat Med* 2018, 24 (7), 908-922.
13. Konerman, M. A.; Jones, J. C.; Harrison, S. A., Pharmacotherapy for NASH: Current and emerging. *J. Hepatol.* 2018, 68 (2), 362-375.
14. Vernon, G.; Baranova, A.; Younossi, Z. M., Systematic review: the epidemiology and natural history of non-alcoholic fatty liver disease and non-alcoholic steatohepatitis in adults. *Aliment Pharmacol Ther* 2011, 34 (3), 274-85.
15. Forman, B. M.; Goode, E.; Chen, J.; Oro, A. E.; Bradley, D. J.; Perlmann, T.; Noonan, D. J.; Burka, L. T.; McMorris, T.; Lamph, W. W.; Evans, R. M.; Weinberger, C., Identification of a Nuclear Receptor That Is Activated by Farnesol Metabolites. *Cell* 1995, 81 (5), 687-693.
16. Sun, L.; Cai, J.; Gonzalez, F. J., The role of farnesoid X receptor in metabolic diseases, and gastrointestinal and liver cancer. *Nat Rev Gastroenterol Hepatol* 2021, 18 (5), 335-347.
17. Potthoff, M. J.; Boney-Montoya, J.; Choi, M.; He, T.; Sunny, N. E.; Satapati, S.; Suino-Powell, K.; Xu, H. E.; Gerard, R. D.; Finck, B. N.; Burgess, S. C.; Mangelsdorf, D. J.; Kliewer, S. A., FGF15/19 regulates hepatic glucose metabolism by inhibiting the CREB-PGC-1alpha pathway. *Cell Metab* 2011, 13 (6), 729-38.
18. Chapman, R. W.; Lynch, K. D., Obeticholic acid-a new therapy in PBC and NASH. *Br Med Bull* 2020, 133 (1), 95-104.
19. Gottlieb, A.; Canbay, A., Why Bile Acids Are So Important in Non-Alcoholic Fatty Liver Disease (NAFLD) Progression. *Cells* 2019, 8 (11).

20. Mudaliar, S.; Henry, R. R.; Sanyal, A. J.; Morrow, L.; Marschall, H. U.; Kipnes, M.; Adorini, L.; Sciacca, C. I.; Clopton, P.; Castelloe, E.; Dillon, P.; Pruzanski, M.; Shapiro, D., Efficacy and safety of the farnesoid X receptor agonist obeticholic acid in patients with type 2 diabetes and nonalcoholic fatty liver disease. *Gastroenterology* 2013, *145* (3), 574-82 e1.
21. Roy, P. P.; Mahtab, M. A.; Rahim, M. A.; Yesmin, S. S.; Islam, S. B.; Akbar, S. M. F., Treatment of Nonalcoholic Steatohepatitis by Obeticholic Acid: Current Status. *EuroAsian J Hepatogastroenterol* 2022, *12* (Suppl 1), S46-S50.
22. Hernandez, E. D.; Zheng, L.; Kim, Y.; Fang, B.; Liu, B.; Valdez, R. A.; Dietrich, W. F.; Rucker, P. V.; Chianelli, D.; Schmeits, J.; Bao, D.; Zoll, J.; Dubois, C.; Federe, G. C.; Chen, L.; Joseph, S. B.; Klickstein, L. B.; Walker, J.; Molteni, V.; McNamara, P.; Meeusen, S.; Tully, D. C.; Badman, M. K.; Xu, J.; Laffitte, B., Tropifexor-Mediated Abrogation of Steatohepatitis and Fibrosis Is Associated With the Antioxidative Gene Expression Profile in Rodents. *Hepatol Commun* 2019, *3* (8), 1085-1097.
23. Wang, Y.; Crittenden, D. B.; Eng, C.; Zhang, Q.; Guo, P.; Chung, D.; Fenaux, M.; Klucher, K.; Jones, C.; Jin, F.; Quirk, E.; Charlton, M. R., Safety, Pharmacokinetics, Pharmacodynamics, and Formulation of Liver-Distributed Farnesoid X-Receptor Agonist TERN-101 in Healthy Volunteers. *Clin Pharmacol Drug Dev* 2021, *10* (10), 1198-1208.
24. Haas, J. T.; Vonghia, L.; Mogilenko, D. A.; Verrijken, A.; Molendi-Coste, O.; Fleury, S.; Deprince, A.; Nikitin, A.; Woittrain, E.; Ducrocq-Geoffroy, L.; Pic, S.; Derudas, B.; Dehondt, H.; Gheeraert, C.; Van Gaal, L.; Driessens, A.; Lefebvre, P.; Staels, B.; Francque, S.; Dombrowicz, D., Transcriptional Network Analysis Implicates Altered Hepatic Immune Function in NASH development and resolution. *Nat Metab* 2019, *1* (6), 604-614.
25. Vuppalauchi, R.; Chalasani, N., Nonalcoholic fatty liver disease and nonalcoholic steatohepatitis: Selected practical issues in their evaluation and management. *Hepatology* 2009, *49* (1), 306-17.
26. Radun, R.; Trauner, M., Role of FXR in Bile Acid and Metabolic Homeostasis in NASH: Pathogenetic Concepts and Therapeutic Opportunities. *Semin Liver Dis* 2021, *41* (4), 461-475.
27. Kim, S. G.; Kim, B. K.; Kim, K.; Fang, S., Bile Acid Nuclear Receptor Farnesoid X Receptor: Therapeutic Target for Nonalcoholic Fatty Liver Disease. *Endocrinol Metab (Seoul)* 2016, *31* (4), 500-504.
28. Sinal, C. J.; Tohkin, M.; Miyata, M.; Ward, J. M.; Lambert, G.; Gonzalez, F. J., Targeted disruption of the nuclear receptor FXR/BAR impairs bile acid and lipid homeostasis. *Cell* 2000, *102* (6), 731-44.
29. Kleiner, D. E.; Brunt, E. M.; Van Natta, M.; Behling, C.; Contos, M. J.; Cummings, O. W.; Ferrell, L. D.; Liu, Y. C.; Torbenson, M. S.; Unalp-Arida, A.; Yeh, M.; McCullough, A. J.; Sanyal, A. J.; Nonalcoholic Steatohepatitis Clinical Research, N., Design and validation of a histological scoring system for nonalcoholic fatty liver disease. *Hepatology* 2005, *41* (6), 1313-21.
30. Loft, A.; Alfaro, A. J.; Schmidt, S. F.; Pedersen, F. B.; Terkelsen, M. K.; Puglia, M.; Chow, K. K.; Feuchtinger, A.; Troullinaki, M.; Maida, A.; Wolff, G.; Sakurai, M.; Berutti, R.; Ekim Ustunel, B.; Nawroth, P.; Ravnskjaer, K.; Diaz, M. B.; Blagoev, B.; Herzig, S., Liver-fibrosis-activated transcriptional networks govern hepatocyte reprogramming and intra-hepatic communication. *Cell Metab* 2021, *33* (8), 1685-1700 e9.
31. Chen, S.; Zhou, Y.; Chen, Y.; Gu, J., fastp: an ultra-fast all-in-one FASTQ preprocessor. *Bioinformatics* 2018, *34* (17), i884-i890.
32. Subramanian, A.; Tamayo, P.; Mootha, V. K.; Mukherjee, S.; Ebert, B. L.; Gillette, M. A.; Paulovich, A.; Pomeroy, S. L.; Golub, T. R.; Lander, E. S.; Mesirov, J. P., Gene set enrichment analysis: a knowledge-based approach for interpreting genome-wide expression profiles. *Proc Natl Acad Sci U S A* 2005, *102* (43), 15545-50.

33. Morrow, M. R.; Batchuluun, B.; Wu, J.; Ahmadi, E.; Leroux, J. M.; Mohammadi-Shemirani, P.; Desjardins, E. M.; Wang, Z.; Tsakiridis, E. E.; Lavoie, D. C. T.; Reihani, A.; Smith, B. K.; Kwiecien, J. M.; Lally, J. S. V.; Nero, T. L.; Parker, M. W.; Ask, K.; Scott, J. W.; Jiang, L.; Pare, G.; Pinkosky, S. L.; Steinberg, G. R., Inhibition of ATP-citrate lyase improves NASH, liver fibrosis, and dyslipidemia. *Cell Metab* 2022, 34 (6), 919-936 e8.
34. Browaeys, R.; Saelens, W.; Saeys, Y., NicheNet: modeling intercellular communication by linking ligands to target genes. *Nat Methods* 2020, 17 (2), 159-162.
35. Govaere, O.; Cockell, S.; Tiniakos, D.; Queen, R.; Younes, R.; Vacca, M.; Alexander, L.; Ravaioli, F.; Palmer, J.; Petta, S.; Boursier, J.; Rosso, C.; Johnson, K.; Wonders, K.; Day, C. P.; Ekstedt, M.; Oresic, M.; Darlay, R.; Cordell, H. J.; Marra, F.; Vidal-Puig, A.; Bedossa, P.; Schattenberg, J. M.; Clement, K.; Allison, M.; Bugianesi, E.; Ratziu, V.; Daly, A. K.; Anstee, Q. M., Transcriptomic profiling across the nonalcoholic fatty liver disease spectrum reveals gene signatures for steatohepatitis and fibrosis. *Sci Transl Med* 2020, 12 (572).
36. Bessone, F.; Razori, M. V.; Roma, M. G., Molecular pathways of nonalcoholic fatty liver disease development and progression. *Cellular and Molecular Life Sciences* 2018, 76 (1), 99-128.
37. Newman, A. M.; Liu, C. L.; Green, M. R.; Gentles, A. J.; Feng, W.; Xu, Y.; Hoang, C. D.; Diehn, M.; Alizadeh, A. A., Robust enumeration of cell subsets from tissue expression profiles. *Nat Methods* 2015, 12 (5), 453-7.
38. Barcena, C.; Stefanovic, M.; Tutusaus, A.; Joannas, L.; Menendez, A.; Garcia-Ruiz, C.; Sancho-Bru, P.; Mari, M.; Caballeria, J.; Rothlin, C. V.; Fernandez-Checa, J. C.; de Frutos, P. G.; Morales, A., Gas6/Axl pathway is activated in chronic liver disease and its targeting reduces fibrosis via hepatic stellate cell inactivation. *J Hepatol* 2015, 63 (3), 670-8.
39. Qing, J.; Ren, Y.; Zhang, Y.; Yan, M.; Zhang, H.; Wu, D.; Ma, Y.; Chen, Y.; Huang, X.; Wu, Q.; Mazhar, M.; Wang, L.; Liu, J.; Ding, B. S.; Cao, Z., Dopamine receptor D2 antagonism normalizes profibrotic macrophage-endothelial crosstalk in non-alcoholic steatohepatitis. *J Hepatol* 2022, 76 (2), 394-406.
40. Han, J.; Zhang, X.; Lau, J. K.; Fu, K.; Lau, H. C.; Xu, W.; Chu, E. S.; Lan, H.; Yu, J., Bone marrow-derived macrophage contributes to fibrosing steatohepatitis through activating hepatic stellate cells. *J Pathol* 2019, 248 (4), 488-500.
41. Li, Y.; Li, M.; Qu, C.; Li, Y.; Tang, Z.; Zhou, Z.; Yu, Z.; Wang, X.; Xin, L.; Shi, T., The Polygenic Map of Keloid Fibroblasts Reveals Fibrosis-Associated Gene Alterations in Inflammation and Immune Responses. *Front Immunol* 2021, 12, 810290.
42. Jiang, J.; Ma, Y.; Liu, Y.; Lu, D.; Gao, X.; Krausz, K. W.; Desai, D.; Amin, S. G.; Patterson, A. D.; Gonzalez, F. J.; Xie, C., Glycine-beta-muricholic acid antagonizes the intestinal farnesoid X receptor-ceramide axis and ameliorates NASH in mice. *Hepatol Commun* 2022, 6 (12), 3363-3378.
43. Younossi, Z. M., Non-alcoholic fatty liver disease - A global public health perspective. *J Hepatol* 2019, 70 (3), 531-544.
44. Adorini, L.; Trauner, M., FXR agonists in NASH treatment. *J Hepatol* 2023.
45. Clifford, B. L.; Sedgeman, L. R.; Williams, K. J.; Morand, P.; Cheng, A.; Jarrett, K. E.; Chan, A. P.; Brearley-Sholto, M. C.; Wahlstrom, A.; Ashby, J. W.; Barshop, W.; Wohlschlegel, J.; Calkin, A. C.; Liu, Y.; Thorell, A.; Meikle, P. J.; Drew, B. G.; Mack, J. J.; Marschall, H. U.; Tarling, E. J.; Edwards, P. A.; de Aguiar Vallim, T. Q., FXR activation protects against NAFLD via bile-acid-dependent reductions in lipid absorption. *Cell Metab* 2021, 33 (8), 1671-1684 e4.

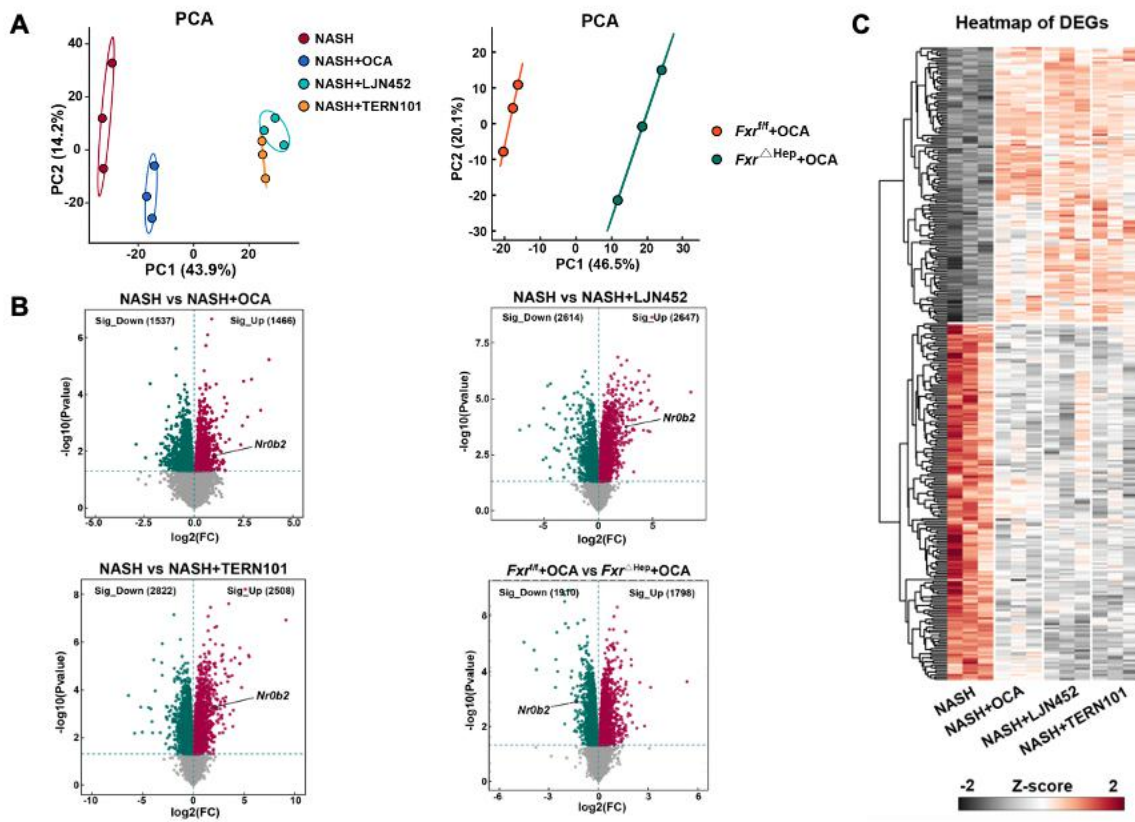
46. Tacke, F.; Puengel, T.; Loomba, R.; Friedman, S. L., An integrated view of anti-inflammatory and antifibrotic targets for the treatment of NASH. *J Hepatol* 2023, **79** (2), 552-566.
47. Powell, E. E.; Wong, V. W.; Rinella, M., Non-alcoholic fatty liver disease. *Lancet* 2021, **397** (10290), 2212-2224.
48. Wu, H.; Liu, G.; He, Y.; Da, J.; Xie, B., Obeticholic acid protects against diabetic cardiomyopathy by activation of FXR/Nrf2 signaling in db/db mice. *Eur J Pharmacol* 2019, **858**, 172393.
49. Huang, F.; Zheng, X.; Ma, X.; Jiang, R.; Zhou, W.; Zhou, S.; Zhang, Y.; Lei, S.; Wang, S.; Kuang, J.; Han, X.; Wei, M.; You, Y.; Li, M.; Li, Y.; Liang, D.; Liu, J.; Chen, T.; Yan, C.; Wei, R.; Rajani, C.; Shen, C.; Xie, G.; Bian, Z.; Li, H.; Zhao, A.; Jia, W., Theabrownin from Pu-erh tea attenuates hypercholesterolemia via modulation of gut microbiota and bile acid metabolism. *Nat Commun* 2019, **10** (1), 4971.
50. Jiang, C.; Xie, C.; Lv, Y.; Li, J.; Krausz, K. W.; Shi, J.; Brocker, C. N.; Desai, D.; Amin, S. G.; Bisson, W. H.; Liu, Y.; Gavrilova, O.; Patterson, A. D.; Gonzalez, F. J., Intestine-selective farnesoid X receptor inhibition improves obesity-related metabolic dysfunction. *Nat Commun* 2015, **6**, 10166.
51. Kuang, J.; Wang, J.; Li, Y.; Li, M.; Zhao, M.; Ge, K.; Zheng, D.; Cheung, K. C. P.; Liao, B.; Wang, S.; Chen, T.; Zhang, Y.; Wang, C.; Ji, G.; Chen, P.; Zhou, H.; Xie, C.; Zhao, A.; Jia, W.; Zheng, X.; Jia, W., Hyodeoxycholic acid alleviates non-alcoholic fatty liver disease through modulating the gut-liver axis. *Cell Metab* 2023.
52. Yan, Y.; Niu, Z.; Sun, C.; Li, P.; Shen, S.; Liu, S.; Wu, Y.; Yun, C.; Jiao, T.; Jia, S.; Li, Y.; Fang, Z. Z.; Zhao, L.; Wang, J.; Xie, C.; Jiang, C.; Li, Y.; Feng, X.; Hu, C.; Jiang, J.; Ying, H., Hepatic thyroid hormone signalling modulates glucose homeostasis through the regulation of GLP-1 production via bile acid-mediated FXR antagonism. *Nat Commun* 2022, **13** (1), 6408.
53. Sanyal, A. J.; Ratziu, V.; Loomba, R.; Anstee, Q. M.; Kowdley, K.; Rinella, M. E.; Sheikh, M. Y.; Trotter, J. F.; Knapple, W.; Lawitz, E. J.; Abdelmalek, M. F.; Newsome, P. N.; Boursier, J.; Mathurin, P.; Dufour, J. F.; Berrey, M. M.; Schiff, S. J.; Sawhney, S.; Capozza, T.; Leyva, R.; Harrison, S. A.; Younossi, Z. M., Results from a new efficacy and safety analysis of the REGENERATE trial of obeticholic acid for treatment of pre-cirrhotic fibrosis due to non-alcoholic steatohepatitis. *Journal of Hepatology* 2023, **79** (5)

SUPPORTING INFORMATION

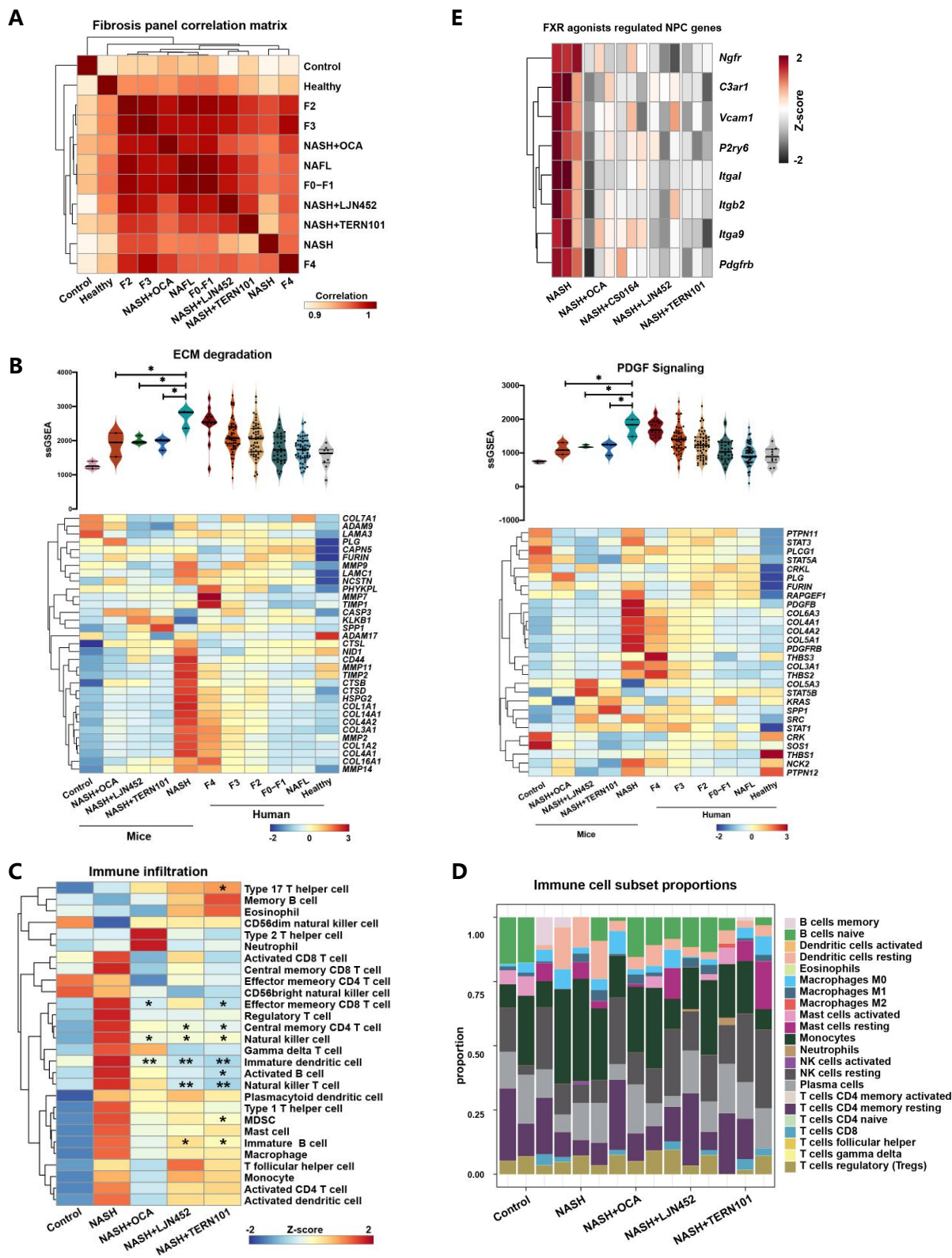


Supporting Fig. S1. Transcriptional characterization of human and mouse NASH at different stages. (A) Liver TG and TC of mice fed GAN diet, n = 5-10/group or GAN diet plus CCl₄, n = 6/group. (B) GSEA of pathways from figure1 and 2. Pathways were split into three clusters by euclidean clustering. Experimental values were presented as mean ± SEM.

*p < 0.05, **p < 0.01, and ***p < 0.001, ns, non-significant.

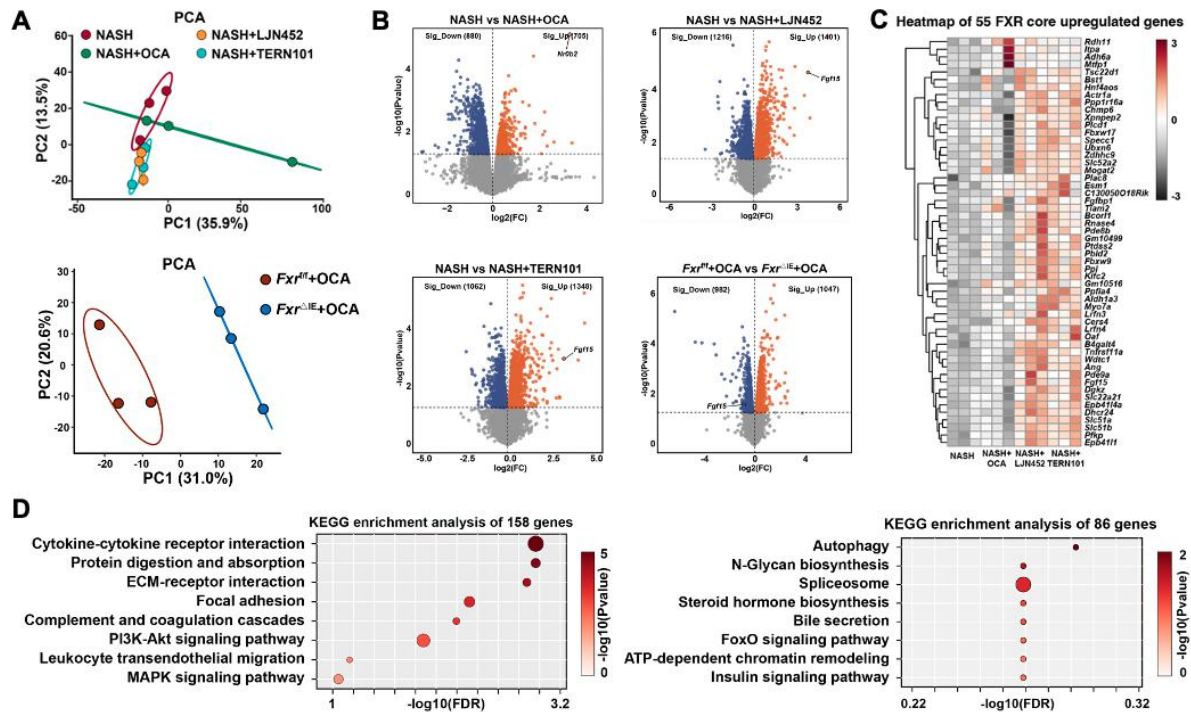


Supporting Fig. S2. Transcriptomic data from the livers of FXR agonist-treated mice. (A) PCA of the RNA-seq data from the liver of mice. (B) Volcano diagram of gene expression from mice treated with different conditions. (C) Heatmap of differentially expressed genes.



Supporting Fig. S3. FXR activation on molecular signatures of inflammation and

fibrosis. (A) Heatmap showing pearson correlation matrix between human and mouse at different NASH stages. (B) Violin plots of ssGSEA scores with accompanying heatmap showing genes expression of indicated pathways in mice and human. Medians, quartiles, max and min are denoted by box plot. (C) ssGSEA heatmap of immune infiltration. (D) Immune infiltration analysis by CIBERSORT showing immune cell subset proportions. (E) Expression heatmap of FXR agonists regulated NPC genes. Experimental values were presented as mean \pm SEM. * $p < 0.05$, ** $p < 0.01$, and *** $p < 0.001$, ns, non-significant.



Supporting Fig. S4. Transcriptomic data from the intestine of FXR agonists treated mice. (A) PCA of the RNA-seq data from the intestine of mice. (B) Volcano diagram of gene expression from mice treated with different conditions. (C) Heatmap of 55 FXR core upregulated genes expression. (D) KEGG enrichment analysis of genes represented FXR agonist benefit.

Tables

Mouse primers	Forward sequence	Reverse sequence
<i>Cyp7a1</i>	AACAAACCTGCCAGTACTAGATAGC	GTGTAGAGTGAAGTCCTCCTTAGC
<i>Cyp8b1</i>	CTAGGGCCTAAAGGTTCGAGT	GTAGCCGAATAAGCTCAGGAAG
<i>Fgf15</i>	GCCATCAAGGACGTCAGCA	CTTCCTCCGAGTAGCGAATCAG
<i>Shp</i>	TCTGCAGGTCGTCCGACTATT	AGGCAGTGGCTGTGAGATGC

Figure legends

FIG. 1. Transcriptomics profiling of livers in humans identifies core NASH transcriptional network. (A) PCA of the RNA-seq data from livers of NASH patients (GSE48452: Control, $n = 14/\text{group}$, Steatosis, $n = 14/\text{group}$, Mild (F0-F1), $n = 14/\text{group}$, Advanced (F2-F4), $n = 4/\text{group}$; GSE130970: Control, $n = 6/\text{group}$, Mild (F0-F1), $n = 45/\text{group}$, Advanced (F2-F4), $n = 25/\text{group}$). (B-C) K-means clustering of row-scaled $\log_2\text{FC}$ in expression of hepatocyte genes differentially expressed ($p < 0.05$) between control, steatosis, mild (F0-F1) and advanced (F2-F4) NASH patients. KEGG enrichment analysis for the indicated clusters. (D-E) GO enrichment analysis of the upregulated clusters (cluster 1, 3, 5 and 7) and the downregulated clusters in NASH patients (cluster 2, 4, 6, and 8).

FIG. 2. Transcriptomics profiling of livers in mice identifies core NASH transcriptional network. (A) Overview of the experimental design of mouse NASH models. (B) Representative H&E and Sirius red stainings of mice fed GAN diet or GAN diet plus CCl₄. Scale bars, 200 μm . (C) PCA of the RNA-seq data from livers of mice from two different NASH models, $n = 3-4/\text{group}$. (D) K-means clustering of row-scaled $\log_2\text{FC}$ in expression of hepatocyte genes differentially expressed ($p < 0.05$) between control, NAFLD, and NASH mice. KEGG enrichment analysis for the indicated clusters. (E-F) GO enrichment analysis of the upregulated clusters (cluster1, cluster3 and cluster5) and the downregulated clusters in NASH mice (cluster2, cluster4 and cluster6).

FIG. 3. Treatment with FXR agonists alleviates NASH-associated phenotypes. (A) Experimental design. (B) Body weight and liver weight. (C) Liver TG, TC and HYP levels. (D) Serum TG, TC, HDL-C, HDL-C, ALT, AST, TBIL and DBIL levels. (E) Expression of FXR target genes in liver and intestine. (F-G) Representative H&E and Sirius red staining of liver sections. Scale bars, 200 μm . Fibrosis score, Sirius red-positive area (%) and NAFLD activity score. Colored bars indicate mean \pm SEM. $n = 5-6/\text{group}$. Different condition groups were compared with NASH+Vehicle group. * $p < 0.05$, ** $p < 0.01$, and *** $p < 0.001$.

FIG. 4. FXR activation reverses the dysregulated core NASH transcriptional network.

(A) Schematic diagram of hepatic RNA sequencing experiment and analysis procedure. (B) PCA of the RNA-seq data from the liver of mice. (C) Heatmap of differentially expressed genes. (D)

Interactive venn diagram. (E) GO enrichment analysis of DEGs. (F) GSEA heatmap of energy metabolism, cell fate, inflammation and fibrosis.

FIG. 5. Machine learning predicts patients' response to treatment of FXR agonists. (A)

PPI network analysis of FXR core upregulated intersection genes. Top 30 hub genes were displayed. (B) Correlation heatmap between top 30 FXR core upregulated genes and biochemical indicators of NASH. (C) PPI network analysis of FXR core downregulated intersection genes. Top 30 hub genes were displayed. (D) Correlation heatmap between top 30 FXR core downregulated genes and biochemical indicators of NASH. (E) Receiver operating characteristic (ROC) curves for NASH stages prediction by three different machine learning methods. (F) Penalty plot of top 30 FXR core upregulated genes and top 30 FXR core downregulated genes in the LASSO model, error bars represent standard error. (G) Top prediction features selected by random forest impurity measurements. (H-I) ssGSEA of NASH-related and FXR core regulated gene set. Using the median as a dividing line. Low, $n = 103/\text{group}$; High, $n = 103/\text{group}$. (J) Receiver operating characteristic (ROC) curves for NASH stages prediction by three different machine learning methods. (K) Interactive venn diagram. (L) Proportion of patients tolerant to FXR agonist therapy and patients sensitive to FXR agonist therapy. $*p < 0.05$, $**p < 0.01$, and $***p < 0.001$.

FIG. 6. Activation of FXR reduces molecular signatures of inflammation and fibrosis.

(A) Gene expression heatmap of 17 orthologous genes identified from the signature genes that characterize NASH severity in humans. (B) PCA coordinate disease progression in human and mice according to average signature gene expression values. (C) GSEA heatmap

of FXR core downregulated pathways. (D) GSEA heatmap of nCounter Fibrosis v2 Panel pathways between mouse cohorts compared to NAFL-F4 stage patients. Pathways are clustered according to pearson correlation and are grouped into clusters I-III. (E) Violin plots showing ssGSEA scores with accompanying heatmaps showing genes expression of indicated pathways in mice and humans. Medians, quartiles, max and min are denoted by box plot. (F) GSEA heatmap of inflammatory pathways associated with fibrosis between mice cohorts. (G) Circle plot showing predicted interaction links between hepatokines (bordeaux) to FXR agonists regulated NPC receptors in macrophage (blue), T cell (orange) and fibroblast (green).

FIG. 7. Activation of intestinal FXR mitigates through the gut-liver axis. (A) Schematic diagram of intestinal RNA sequencing experiment and analysis procedure. (B) Interactive venn diagram. (C) GO enrichment analysis of instinal FXR core upregulated genes. (D) Heatmap of DEGs expression and GO enrichment analysis of instinal FXR core downregulated genes. (E) GSEA heatmap of bile acid and inflammation pathways. (F) Volcano plot showing DEGs from liver. Fxr^{ff} vs $Fxr^{\Delta E}$, Control vs NASH (GAN diet), and Control vs NASH (GAN diet + CCl₄), p<0.05. (G) Interactive venn diagram. Genes representing FXR agonist benefit and FXR inhibitor benefit. (H) GO enrichment analysis of genes represented FXR inhibitor benefit. (I) GO enrichment analysis of genes represented FXR agonist benefit.

Figure 1 Transcriptomics profiling of livers in humans identifies core NASH transcriptional network

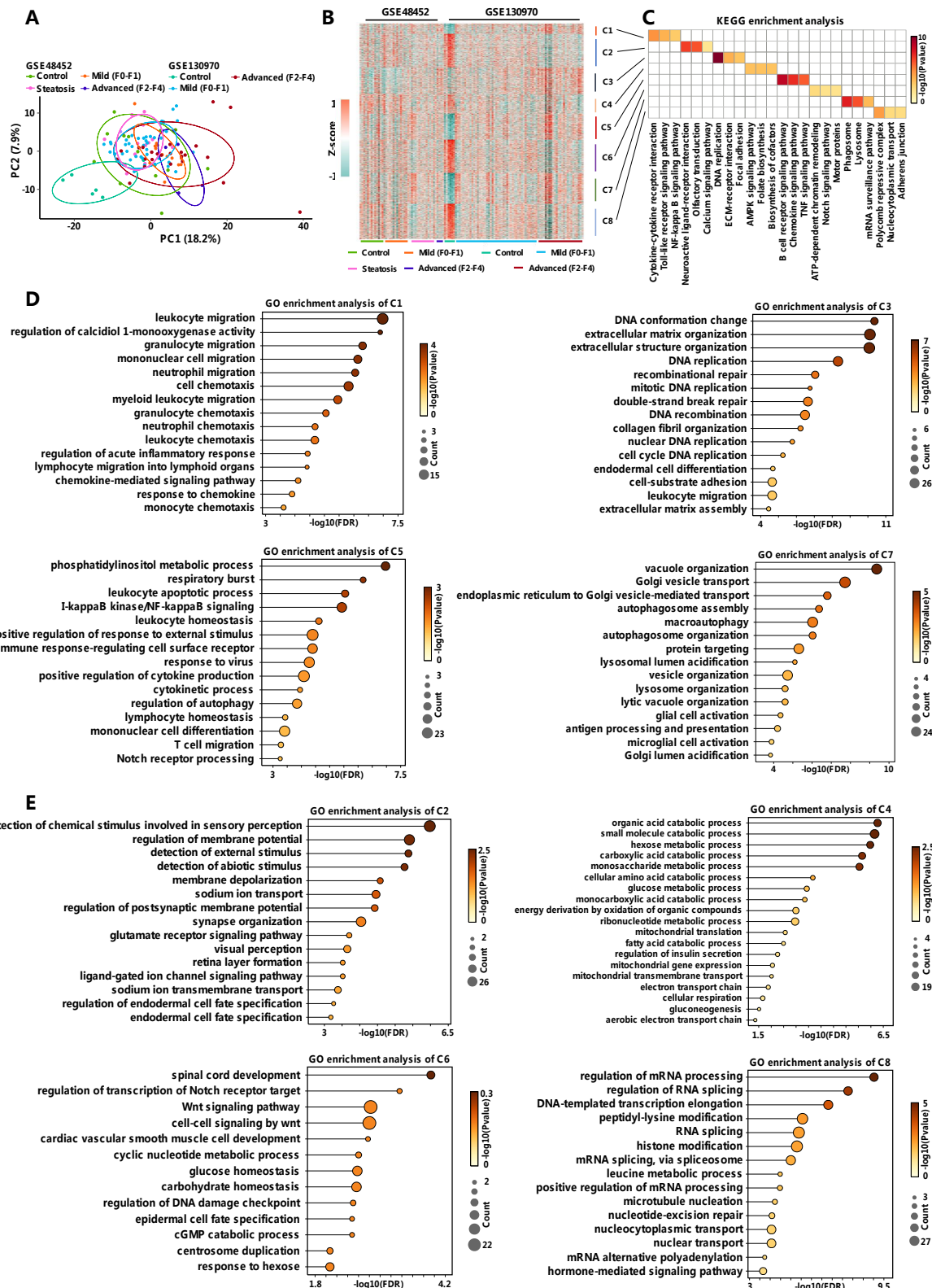


Figure 2. Transcriptomics profiling of livers in mice identifies core NASH transcriptional network

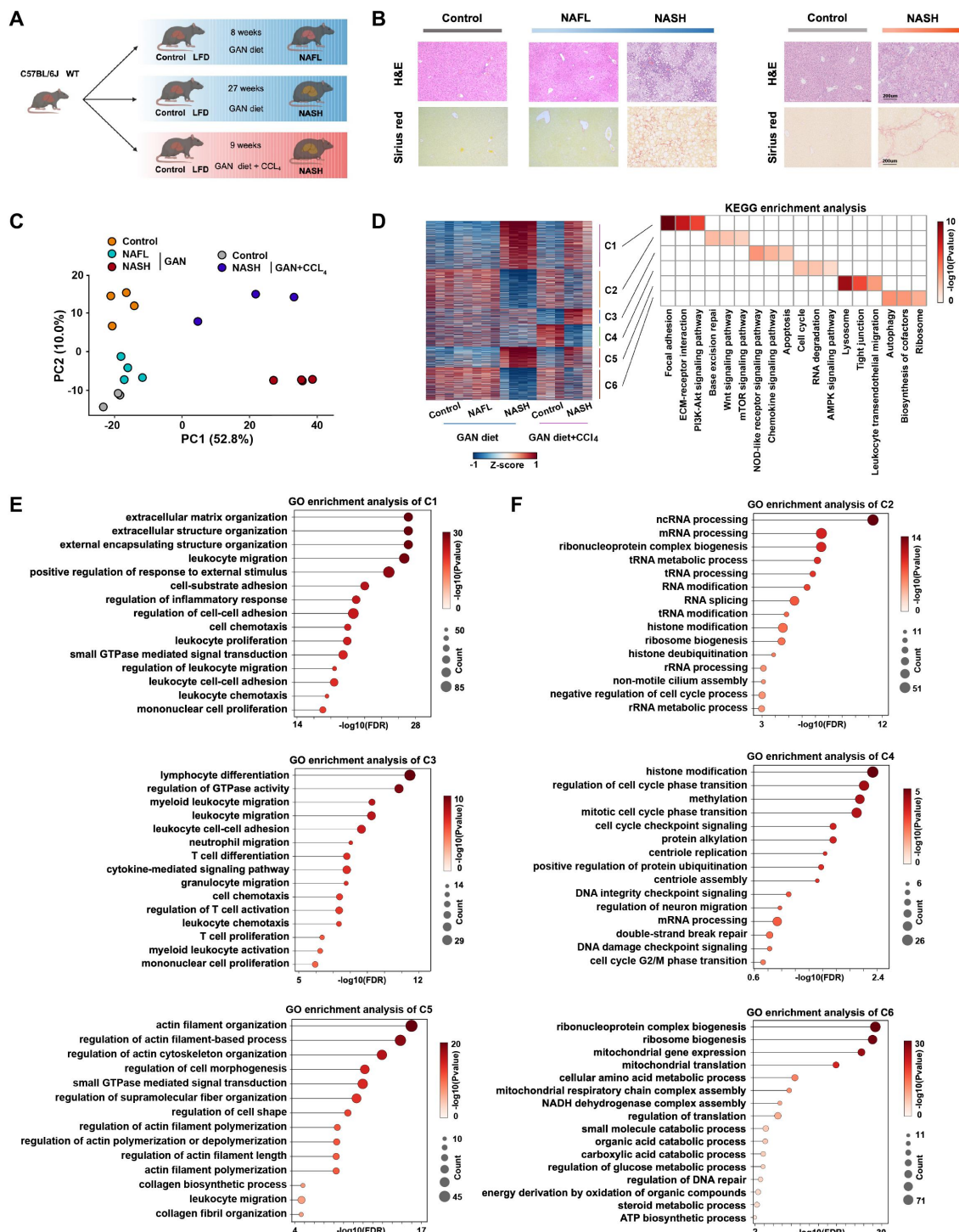


Figure 3. Treatment with FXR agonists alleviates NASH-associated phenotypes

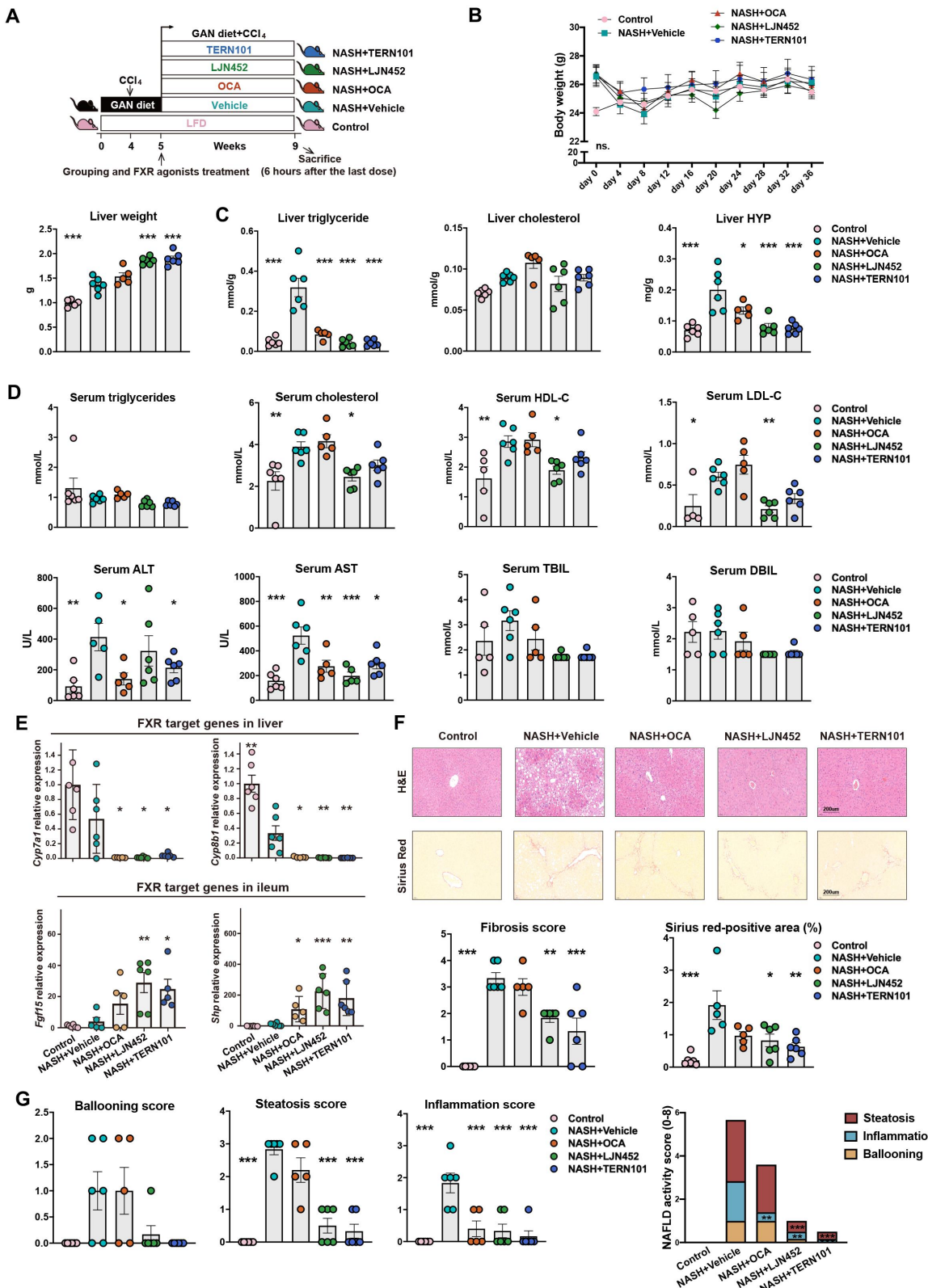


Figure 4. FXR activation reverses the dysregulated core NASH transcriptional network

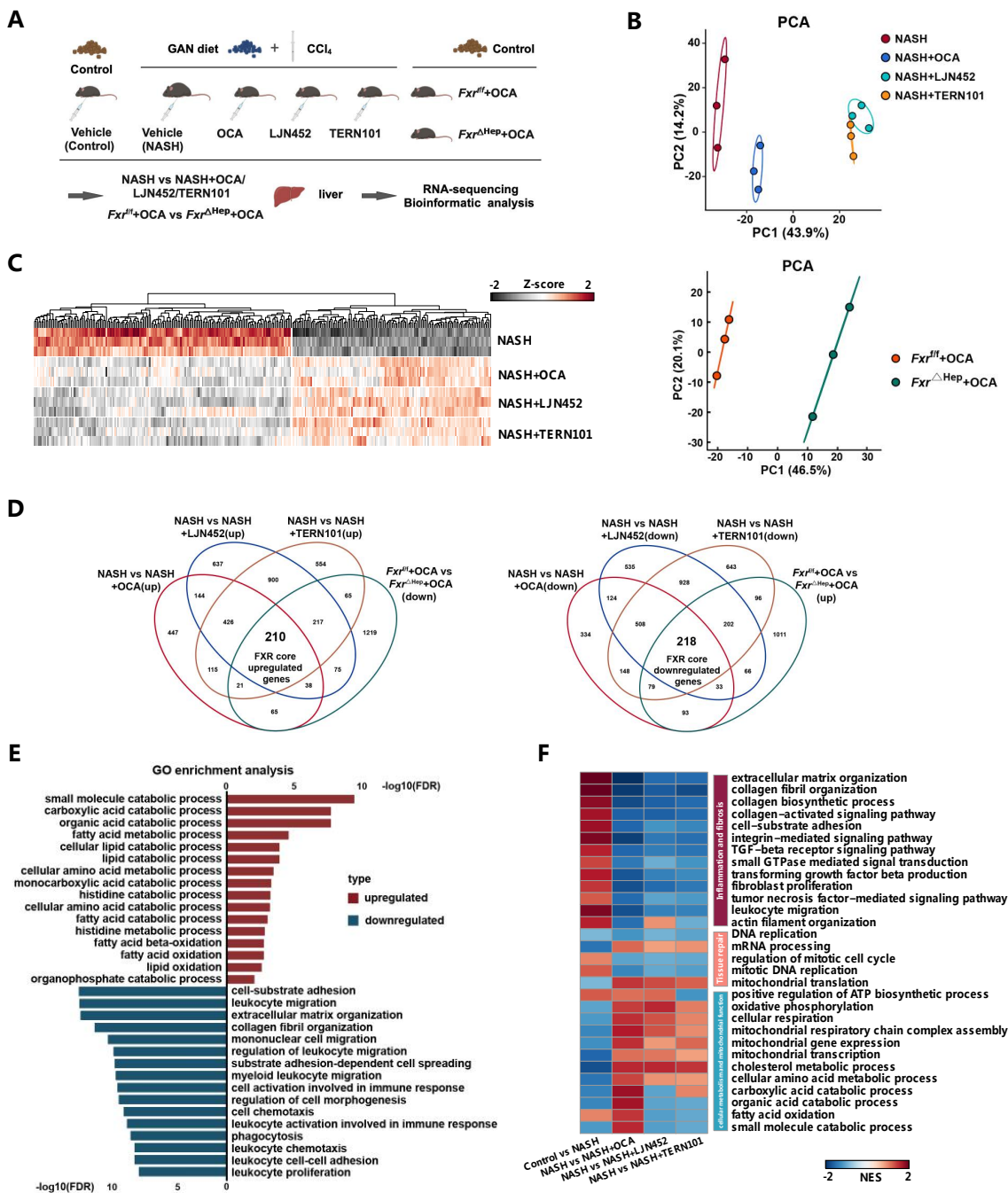


Figure 5. Machine learning predicts patients' response to treatment of FXR agonists

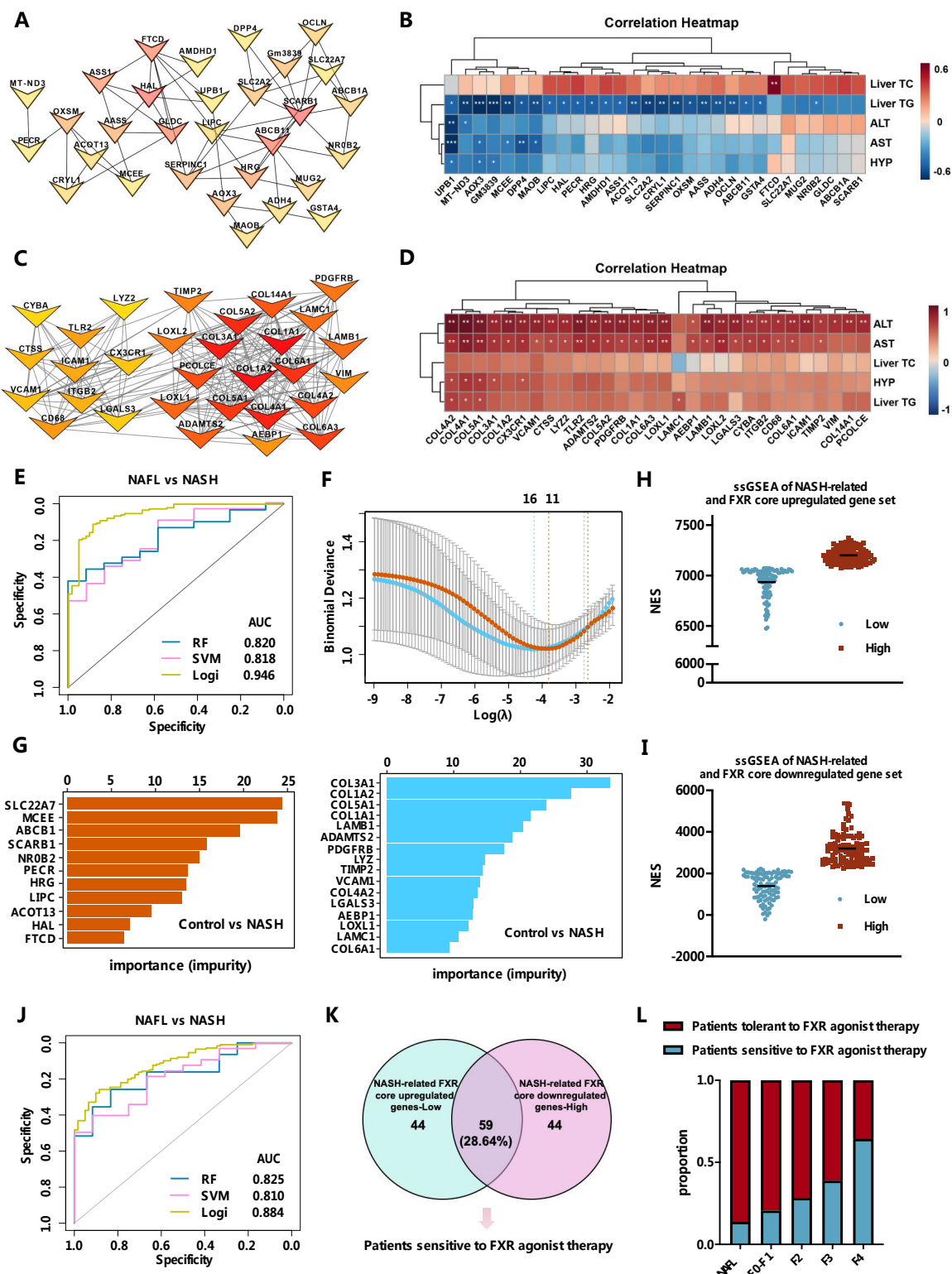


Figure 6. Activation of FXR reduces molecular signatures of inflammation and fibrosis

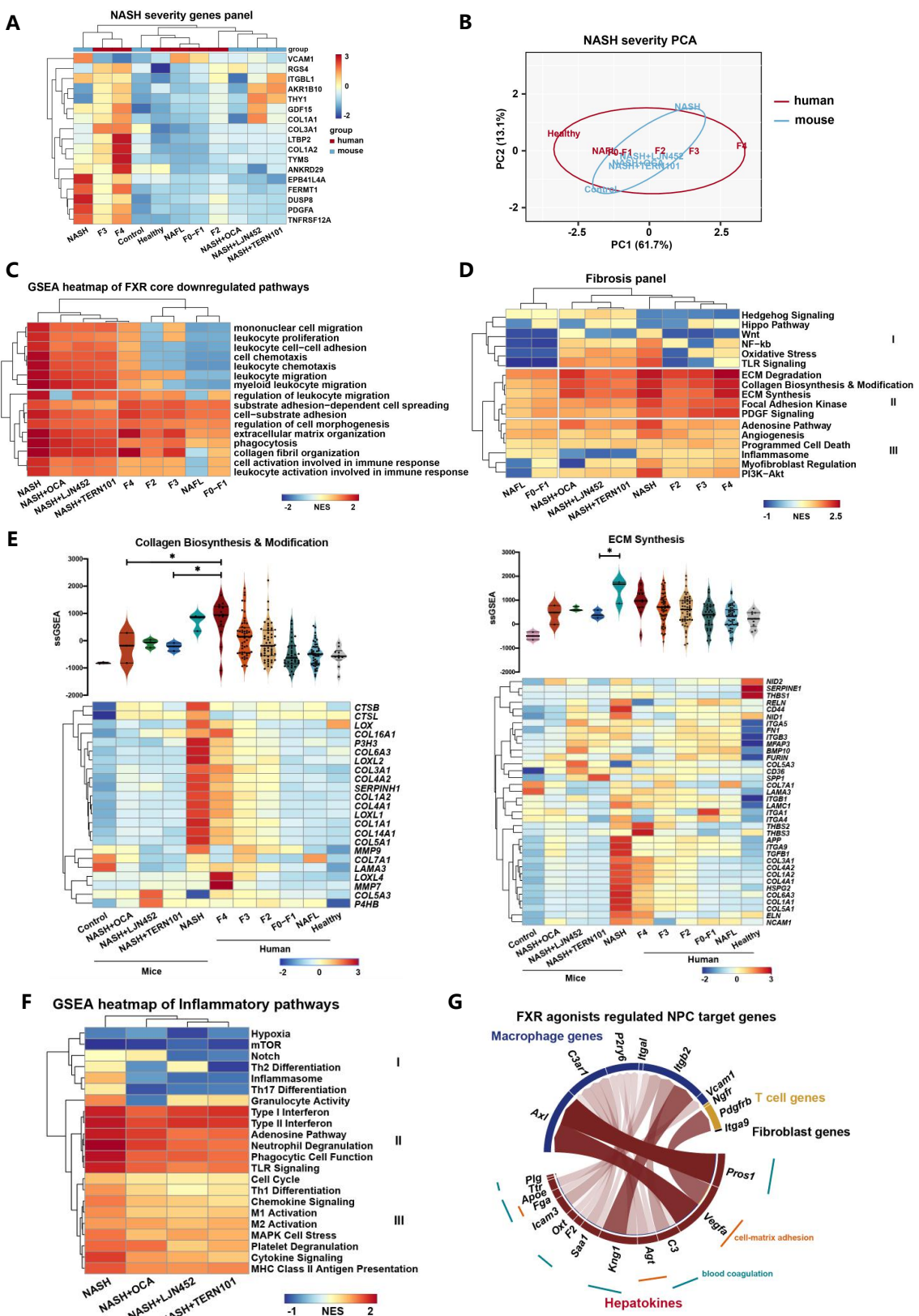


Figure 7. Activation of intestinal FXR mitigates through the gut-liver axis

